  Bull. Chem. Soc. Jpn., 65, 373—384 (1992)

Hydrolytic Metalloenzyme Models. Metal Ion Dependent Site-Selective Acylation of Hydroxyl Groups of Bis-Imidazole Ligands Catalyzed by Zn^{2+} and Cu^{2+} in the Reaction with *p*-Nitrophenyl 2-Pyridinecarboxylate in a Cationic Surfactant Micelle

Kenji OGINO, Nobuyuki KASHIHARA, Toshitomo UEDA, Toshihide ISAKA, Toshiharu YOSHIDA, and Waichiro TAGAKI*

Department of Bioapplied Chemistry, Faculty of Engineering, Osaka City University, Sugimoto 3-3-138, Sumiyoshi-ku, Osaka 558

(Received September 13, 1991)

Co-micelles of hexadecyltrimethylammonium bromide and a lipophilic bis-imidazole ligand, 1-dodecyl-4-hydroxymethyl-α-(1-dodecyl-2-imidazolyl)-2-imidazolemethanol (**4**) having two primary and secondary hydroxyl groups, together with the co-micelles of the related lipophilic ligands, were investigated for their catalytic activities in the hydrolysis of *p*-nitrophenyl 2-pyridinecarboxylate (PNPP) in the presence of Zn^{2+} or Cu^{2+}. The kinetic and product analyses indicated that the reaction proceeds through the transacylation from PNPP to the hydroxyl group of ligand : metal ion complexes and that the active complexes undergoing transacylation are a 2 : 1 and a 1 : 1 complex for Zn^{2+} and a 1 : 1 complex for Cu^{2+}, respectively. As for the ligand **4**, the transacylation was found to be highly site-selective, i.e. it occurred predominantly on the secondary hydroxyl group with Zn^{2+}, while on the primary hydroxyl group with Cu^{2+}, respectively. Such selectivity was discussed in terms of the coordination structures of the active complexes.

The catalytic activities of metalloenzymes are known to be dependent on metal ion species. For example, in carboxypeptidase A (CPA), a Zn^{2+}-containing proteolytic enzyme, the activity change is small when Zn^{2+} is replaced with Co^{2+} or Ni^{2+}, but when replaced with Cu^{2+} the enzyme becomes totally inactive toward peptide and ester substrates.[1] A geometrical distortion is presumed to be one important factor for the loss of activity in Cu^{2+}/CPA. Metal ion effects have also been studied for other zinc-enzymes such as alkaline phosphatase[2] and carbonic anhydrase,[3] and a tetrahedral coordination of Zn^{2+} with imidazole ligands is considered to be important for the generation of full enzymic activity in such enzymes.

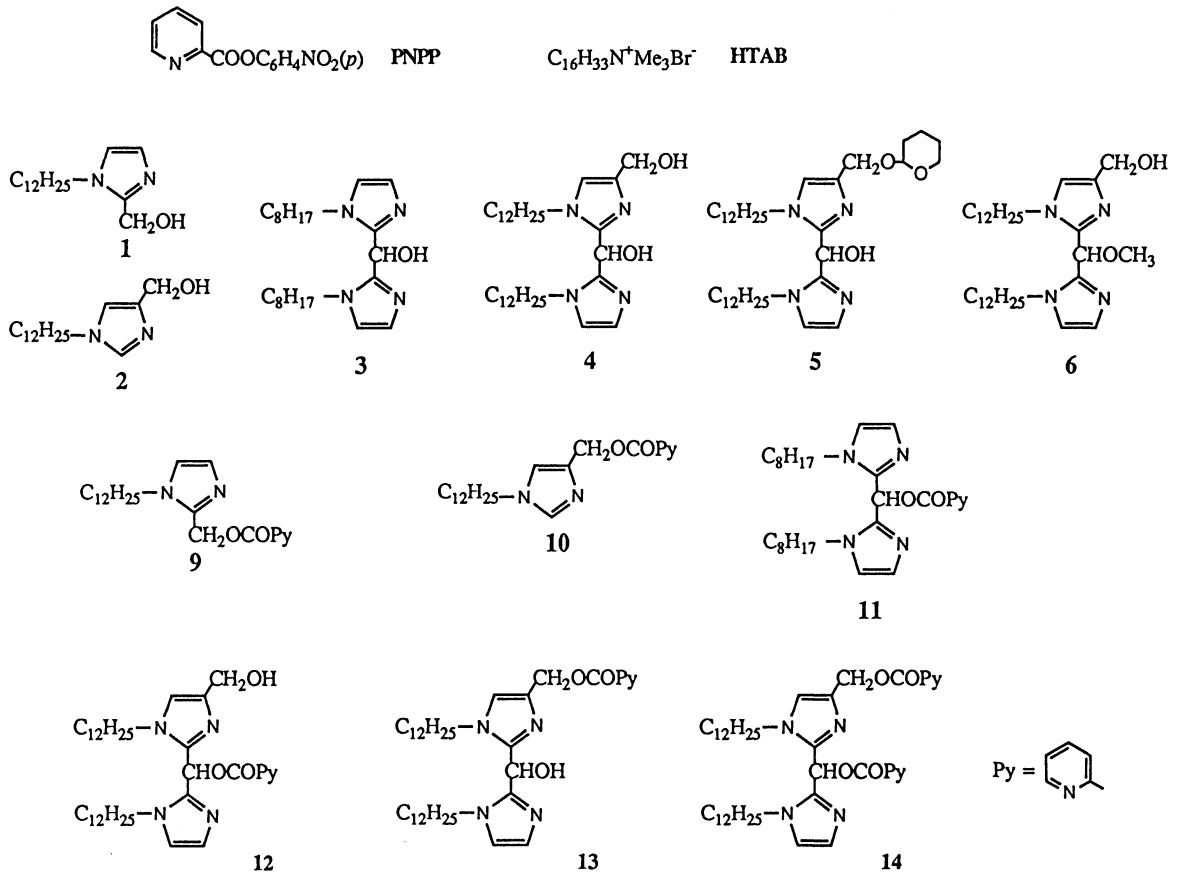

The roles of Zn^{2+} in the catalytic activities of the above mentioned enzymes have been the subject of extensive model studies. One obvious role of a metal ion is to function as an electrophilic catalyst, stabilizing the negative charges that are formed during the reaction.[4] In CPA, the Zn^{2+} at the active site of enzyme coordinates to the carbonyl oxygen of an amide substrate, assisting it to undergo nucleophilic attack, and stabilizes the tetrahedral intermediate by an electrostatic interaction. Another important function of a metal ion is to play as a source of hydroxide ion at neutral pH. It is not uncommon that a metal-bound water molecule ionizes with a pK_a near 7, about 9 units below that of free water, yielding a high fraction of coordinated hydroxide ion at neutral pH. Moreover, such a metal-bound hydroxide ion is a potent nucleophile retaining most of the reactivity of free hydroxide ion.[4-6] These metal ion functions are quite attractive for the design of artificial hydrolytic metalloenzymes as exemplified in a number of non-micellar[7,8] and micellar[9-14] models. However, the information has been limited as for the active geometries of metal ion coordination in such model studies except for in several cases.[8]

Previously, we reported that the metal ion complexes of 1-dodecyl-2-hydroxymethylimidazole/Cu^{2+} (**1**·Cu^{2+})[9,13] and bis(1-octyl-2-imidazolyl)methanol/Zn^{2+} (**3**·Zn^{2+})[9] are remarkably active catalysts for the hydrolysis of *p*-nitrophenyl 2-pyridinecarboxylate (PNPP) when used as the co-micelles of hexadecyltrimethylammonium bromide (HTAB). It was later noticed that the activation of the former mono-imidazole ligand by Zn^{2+} and of the latter bis-imidazole ligand by Cu^{2+} is surprisingly small. These observations suggest that Zn^{2+} and Cu^{2+} activate the ligand hydroxyl group by different modes of complexation.

In order to obtain more convincing information on the difference between Zn^{2+} and Cu^{2+} in the activation of ligands, some lipophilic bis-imidazole ligands; 1-dodecyl-4-hydroxymethyl-α-(1-dodecyl-2-imidazolyl)-2-imidazolemethanol (**4**) having two primary and secondary hydroxyl groups and its tetrahydropyranyl- **5** and methyl ether **6** have been prepared and their catalytic activities for the hydrolysis of PNPP have been examined in the presence of Zn^{2+} and Cu^{2+} and compared with those of the reported ligands **1**—**3**.[9-13,15] These bis-imidazole ligands are able to take two different forms according to the CPK molecular models, i.e. a tetrahedral and a square planar forms in complexation with a metal ion. Interesting possibilities are that the former tetrahedral complexation would activate the secondary hydroxyl group and the latter square planar one would activate the primary hydroxyl group toward the transacylation.

Results and Discussion

Preparation of Ligands. The ligands **1**, **2**, and **3** were prepared according to the previous methods.[9-11] The bis-imidazole ligands **4**, **5**, and **6** were prepared according to the procedures shown in Scheme 1. All ligands **1**—**6** were practically insoluble in aqueous media, but could be solubilized in the aqueous micellar solutions of HTAB.

A Survey of Rates at pH 7.05. The kinetics were carried out in buffered micellar solutions of HTAB. The rates of hydrolyses were determined by monitoring the release of *p*-nitrophenol from the substrate PNPP spectrophotometrically as reported previously.[13] In Table 1 are shown the pseudo-first-order rate constants (k_{obsd}) obtained under the conditions of an excess ligand

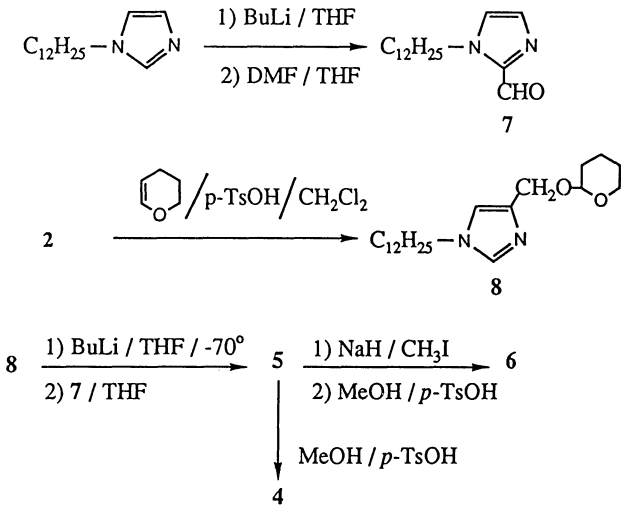

Scheme 1. Preparation of lipophilic ligands.

Table 1. Pseudo-First-Order Rate Constants (k_{obsd}) for the Release of *p*-Nitrophenol from PNPP at pH 7.05, 25 °C[a]

Run	Ligand	Metal ion	$k_{obsd}\times10^{2}$ [b]
	mol dm^{-3}	mol dm^{-3}	s^{-1}
1	None	None	0.00193
2	None	Zn^{2+} (1×10^{-3})	0.028
3	None	Cu^{2+} (1×10^{-4})	3.78
4	**1** (2×10^{-4})	None	0.192
5	**1** (2×10^{-4})	Zn^{2+} (1×10^{-3})	3.02
6	**1** (5×10^{-4})	Zn^{2+} (1×10^{-3})	9.22
7	**1** (1×10^{-4})	Cu^{2+} (1×10^{-4})	491
8	**2** (5×10^{-4})	Zn^{2+} (1×10^{-3})	4.22
9	**2** (5×10^{-5})	Cu^{2+} (1×10^{-4})	185
10	**3** (2×10^{-4})	None	0.307
11	**3** (2×10^{-4})	Zn^{2+} (1×10^{-3})	41.5
12	**3** (5×10^{-5})	Cu^{2+} (1×10^{-4})	15.3
13	**4** (2×10^{-4})	Zn^{2+} (1×10^{-3})	25.4
14	**4** (5×10^{-5})	Cu^{2+} (1×10^{-4})	195
15	**5** (5×10^{-5})	None	0.053
16	**5** (2×10^{-4})	Zn^{2+} (1×10^{-3})	25.1
17	**5** (5×10^{-5})	Cu^{2+} (1×10^{-4})	18.3
18	**6** (5×10^{-5})	None	0.014
19	**6** (2×10^{-4})	Zn^{2+} (1×10^{-3})	1.87
20	**6** (5×10^{-5})	Cu^{2+} (1×10^{-4})	115

a) The uncatalyzed non-micellar rate was 1.67×10^{-5} s^{-1}.
b) All in the presence of [HTAB] $=1\times10^{-2}$ mol dm^{-3}.

and metal ion over the substrate at constant pH 7.05 and 25 °C.

Table 1 indicates that the rate enhancing micellar effect of HTAB itself (1.93×15^{-5} s^{-1}, Run 1) is negligibly small as compared to the uncatalyzed rate (1.67×10^{-5} s^{-1}). As expected, Zn^{2+} and Cu^{2+}, in particular the latter, showed reasonable rate enhancing effects (Runs 2 and 3). Every ligand solubilized in HTAB micelle showed some enhanced reactivities (Runs 4, 10, 15, and 18). However, it can be seen in Table 1 that the co-existence of a metal ion and a ligand is essential for a remarkable rate enhancement. In the cases of Zn^{2+}, the rate enhancement was particularly large with the ligands, **3**, **4**, and **5** which are all bis-imidazole ligands having free secondary hydroxyl groups (Runs 11, 13, and 16). It is important to notice that the activity of **6**·Zn^{2+} is small, in which the secondary hydroxyl group is blocked by methyl group although the primary hydroxyl group is in free state (Run 19). On the other hand, the activation by Cu^{2+} was particularly large with the ligands, **1**, **2**, **4**, and **6** which all have a free primary hydroxyl group (Runs 7, 9, 14, and 20), in contrast to a relatively small activation with the ligands, **3** and **5** which do not have a free primary hydroxyl group (Runs 12 and 17). Thus a rate enhancement of 2.2×10^4 fold was obtained in the presence of 2×10^{-4} mol dm^{-3} of **3** and 1×10^{-3} mol dm^{-3} of Zn^{2+} (Run 11). Likewise, a rate enhancement of 10^5 fold was obtained in the presence of 5×10^{-5} mol dm^{-3} of **4** and 1×10^{-4} mol dm^{-3} of Cu^{2+} (Run 14). As described below, the rate enhancement is due to the activation of ligand hydroxyl groups as nucleophiles by the coordinated metal ions. In this regards, it was confirmed that the ligands having no hydroxyl group show only negligible activities.

Reaction Schemes and the Rate Equations. The above mentioned rates were dependent on each concentration of metal ion, ligand, HTAB, and on pH. As for HTAB, its concentration effect on the rate was already examined for the **1**·Cu^{2+} complex:[13] i.e. there was observed a typical rate enhancing micellar effect by increasing HTAB concentration up to 5×10^{-3} mol dm^{-3} followed by a rate saturation. Accordingly, a constant concentration of [HTAB]$=1\times10^{-2}$ mol dm^{-3} was used throughout this investigation as an enough concentration for both the solubilization of a lipophilic ligand and the rate saturation.

As reported previously,[9,13] it is reasonable to assume a reaction scheme 2 involving Eqs. 1—3. The scheme indicates that a metal ion (M) forms a complex (M-L_n) with n ligands (L) with an association constant (K_M) (Eq. 1), and that the complex reacts with the substrate (S) bimolecularly in the rate-limiting step with an apparent second-order rate constant (k_N') to afford the products (P) (Eq. 2). The products are also formed through k_o' process without involving an M-L_n complex (Eq. 3). An alternative scheme involving a ternary complex, S·M·L_n, may well be considered. The choice of Eq. 2 in Scheme 2 instead of such a ternary complex is simply due to the consideration that the substrate pyridine moiety should be weak as a ligand base in the ground state in aqueous buffers, although it becomes effective upon the formation of a tetrahedral addition intermediate (see the later discussion).

$$M + nL \overset{K_M}{\rightleftharpoons} M\text{-}L_n;\ K_M = [M\text{-}L_n]/[M][L]^n \quad (1)$$

$$S + M\text{-}L_n \xrightarrow{k_N'} P \quad (2)$$

$$S \xrightarrow{k_o'} P \quad (3)$$

Scheme 2.

$$\text{Rate} = k_{obsd}[S] = (k_o' + k_1[M\text{-}L] + k_2[M\text{-}L_2])[S] \quad (4)$$

$$k_o' = k_o + k_L[L]_T + k_M[M]_T \quad (5)$$

One must also consider that the reaction mixture consists of a mixture of complexes, and for each complex the Eqs. 1 and 2 holds. Thus the rate of reaction is represented by Eqs. 4 and 5, where M-L and M-L_2 are 1 : 1 (n=1) and 2 : 1 (n=2) complexes of the ligand and the metal ion, respectively, with the corresponding rate constants, k_1 and k_2. The k_o' in Eq. 5 consists of the rate constants due to the other than M-L_n, where $[L]_T$ and $[M]_T$ are the total concentrations of the ligand and the metal ion, respectively. Here the other higher order complexes, such as M-L_3 or M_2L_2 etc. are neglected based on the experimental observations on the effects of metal ion concentration on the rates. Even with a mixture of M-L and M-L_2, the analysis of the observed rates (k_{obsd}) would become complicating if both complexes are comparable in the rates. However, as described below, it was able to select the experimental conditions under which the k_1 process of M-L is more important than the k_2 process of M-L_2.

(a) Job Plots: Normally, n value in Eq. 1 is esti-

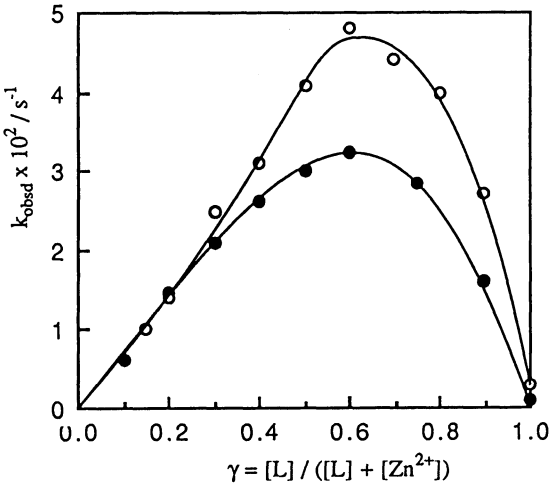

Fig. 1. Job plots for the hydrolysis of PNPP in the presence of ligand **3** (○) or **4** (●) and Zn^{2+} in HTAB micelles, pH 7.03, 25 °C: [L]+[Zn^{2+}]$=1\times10^{-4}$ mol dm^{-3}, [PNPP]$=1\times10^{-4}$ mol dm^{-3}, [HTAB]$=1\times10^{-2}$ mol dm^{-3}.

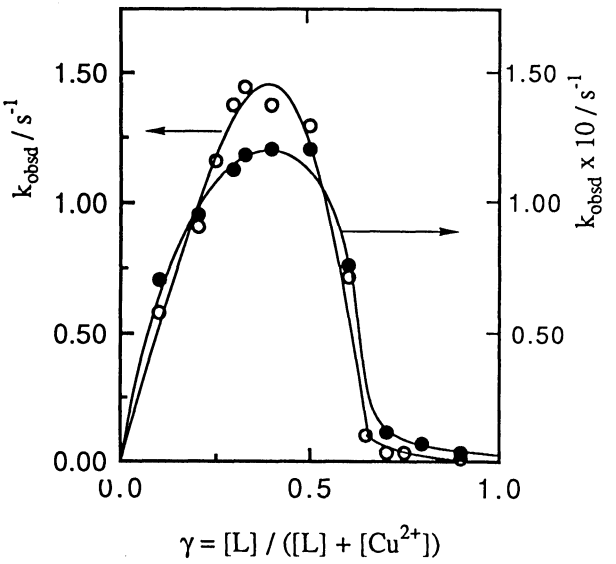

Fig. 2. Job plots for the hydrolysis of PNPP in the presence of ligand **3** (●) or **4** (○) and Cu^{2+} in HTAB micelles, pH 7.03, 25 °C: [L]+[Cu^{2+}]=1×10^{-4} mol dm^{-3}, [PNPP]=1×10^{-4} mol dm^{-3}, [HTAB]=1×10^{-2} mol dm^{-3}.

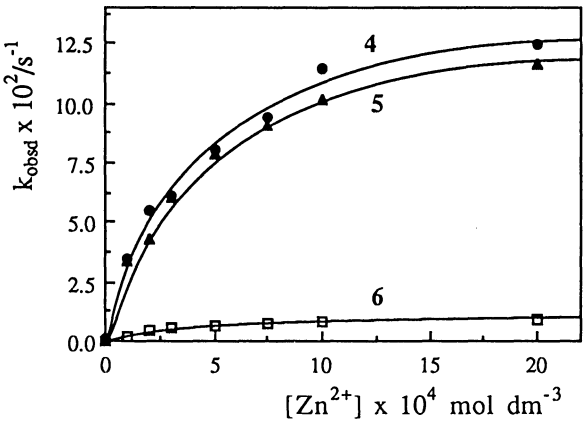

Fig. 3. Plots of k_{obsd} vs. Zn^{2+} concentration for *p*-nitrophenol release from PNPP in HTAB micelles under fixed concentrations of [PNPP]=1×10^{-5}, [ligand]=5×10^{-5}, and [HTAB]=1×10^{-2} mol dm^{-3}; pH 7.03, 25 °C.

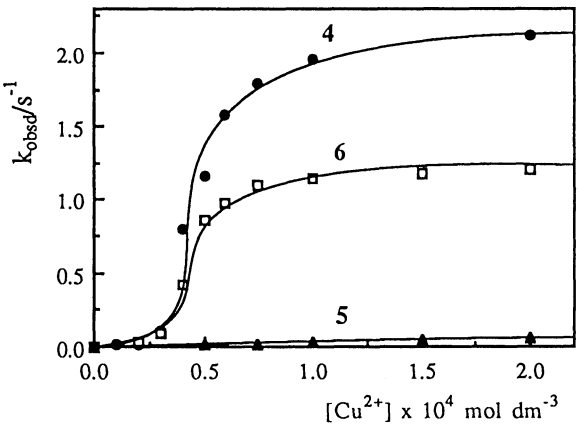

Fig. 4. Plots of k_{obsd} vs. Cu^{2+} concentration for *p*-nitrophenol release from PNPP in HTAB micelles under fixed concentrations of [PNPP]=1×10^{-5}, [ligand]=5×10^{-5}, and [HTAB]=1×10^{-2} mol dm^{-3}; pH 7.03, 25 °C.

mated by the kinetic version of Job plots,[16] in which the rate constants are plotted as a function of the mole fraction of a ligand or metal ion, keeping their total concentration being constant. The representative results taking the ligands **3** and **4** as the examples are shown in Figs. 1 and 2. Both figures indicate the necessity of coexistence of the ligand and the metal ion to attain higher rates (k_{obsd}). They also indicate the existence of an optimum γ value to attain a maximum rate. For the cases of Zn^{2+} in Fig. 1, the maximum rates are seen at the position between γ=0.5 and 0.67, corresponding to the γ values for a 1 : 1 (n=1) and a 2 : 1 (n=2) complexes, respectively. Apparently for Zn^{2+} and for both **3** and **4**, both M–L and M–L_2 complexes are important for the rate enhancement under the conditions of Job plots. For the cases of Cu^{2+} in Fig. 2, the shapes of two curves are widely different from those in Fig. 1, i.e. the rate maxima are seen at the neighborhood of γ=0.4, and then the rates drop sharply to almost negligible values with increasing γ values. These results suggest that in the case of Cu^{2+} the active complex is M–L (n=1), while the M–L_2 complex is inactive.

(b) Saturation Kinetics: Dependency of Rates on the Metal Ion Concentration: The dependency of rates on the metal ion concentration are shown in Figs. 3 and 4. Figure 3 indicates that for each of the three ligands the rate increased with increasing Zn^{2+} concentration up to a saturation level. It is important to notice that such activation of a ligand by Zn^{2+} is remarkably large with the ligands **4** and **5** having a free secondary hydroxyl group, but not with the ligand **6** in which the secondary hydroxyl group is blocked with methyl group although the primary hydroxyl group is left free. Figure 4 indicates that the sigmoidal curves were observed in the activation by Cu^{2+} for the ligands **4** and **6** having a free primary hydroxyl group, i.e. the activation is negligible at first when the Cu^{2+} concentration is below a half that of ligand, but above it the activation becomes remarkably large. These sigmoidal dependencies of rates on the Cu^{2+} concentrations are consistent with the results of Job plots in Fig. 2. Figure 4 also indicates that the activation by Cu^{2+} is very small for the ligand **5** in which the primary hydroxyl group is blocked with a tetrahydropyranyl group although the secondary hydroxyl group is left free. These results clearly indicate that Zn^{2+} activates the secondary hydroxyl group and Cu^{2+} activates the primary hydroxyl group, both in a highly site-selective manner. Thus the ligand **4** having both free primary and secondary hydroxyl groups can be activated by both Cu^{2+} and Zn^{2+}.

(3) Kinetic Analyses: (i) Zn^{2+} Catalysis. As men-

tioned above, the contribution of the Zn^{2+}–L_2 complex (n=2) on the rate cannot be neglected under the conditions of an excess ligand over Zn^{2+} (e.g. the rates in the right side portion of the Job plots in Fig. 1). However, the Zn^{2+}–L complex (n=1) should become more important than the Zn^{2+}–L_2 complex under the conditions of an excess Zn^{2+} over the ligand (e.g. the rates in the left side portion of the Job plots in Fig. 1 and the most of the rates in Fig. 3).

When the M–L_2 complex is neglected, Eq. 4 can be simplified to Eq. 6 which leads to Eqs. 7, 8, where K_M is an association constant of M–L complex and the other terms are the same as defined above in Eqs. 4 and 5, where $k_1'=k_N'$. Actually, all the Zn^{2+}-catalyzed k_{obsd} values observed for the ligands **3**, **4**, **5**, and **6** could be analyzed based on these equations. Representative data obtained for the ligand **4** are shown in Figs. 5—8. Reciprocal plots in Fig. 6 based on Eq. 8 allowed to obtain intercepts and slopes as the function of $[L]_T$. Figure 7 indicates a linear plot between the 1/intercept's and $[L]_T$'s which allowed to calculate the k_N' value. Similarly, Fig. 8 indicates a linear plot between the slopes and $1/[L]_T$'s which allowed to calculate the K_M' value. Finally, these k_N' and K_M' values allowed to reproduce the saturation curves in Fig. 5. It should be mentioned that these k_N' and K_M' values are pH dependent as described later.

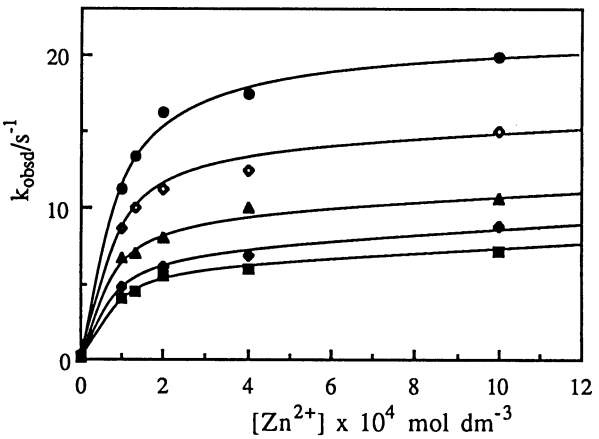

Fig. 5. Plots of k_{obsd} vs. Zn^{2+} concentration for p-nitrophenol release from PNPP in HTAB micelles (1×10^{-2} mol dm^{-3}), pH 7.03, 25 °C: ligand **4** concentrations are 3.0, 2.0, 1.5, 1.2, 1.0×10^{-4} mol dm^{-3} from the top curve.

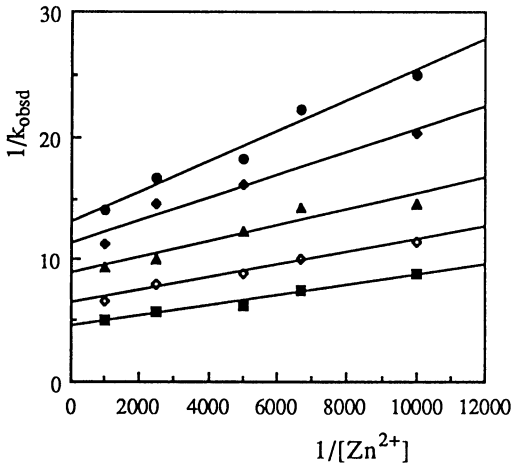

Fig. 6. Plots of $1/k_{obsd}$ vs. $1/[Zn^{2+}]$ derived from the plots in Fig. 5.

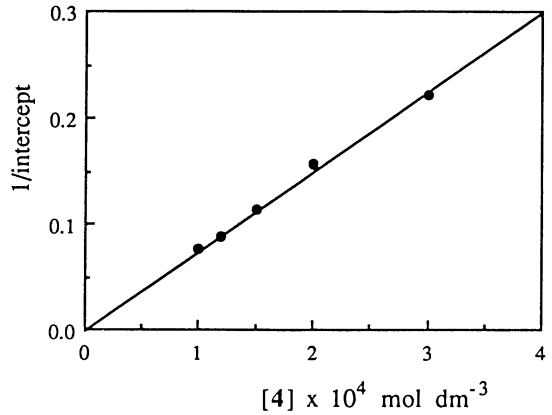

Fig. 7. Plots of 1/intercept vs. [**4**] derived from the plots in Fig. 6.

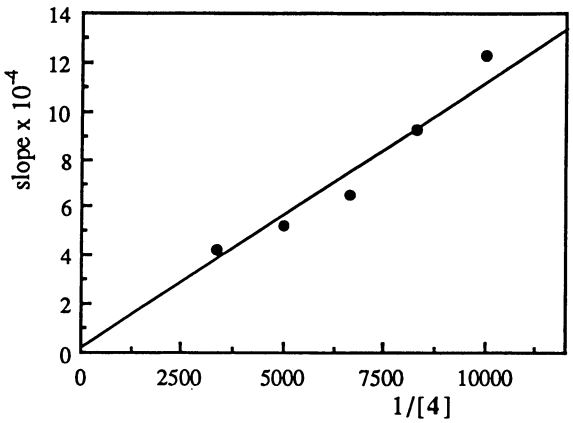

Fig. 8. Plots of slope vs. 1/[**4**] derived from the plots in Fig. 6.

$$\text{Rate} = k_{obsd}[S] = (k_0' + k_N'[M\text{-}L])[S] \quad (6)$$

$$k_{obsd} = k_0' + \frac{k_N' K_M' [L]_T [M]_T}{1 + K_M'([L]_T + [M]_T)} \quad (7)$$

$$\frac{1}{(k_{obsd} - k_0')} = \frac{1}{k_N'[L]_T} + \frac{1 + K_M'[L]_T}{k_N' K_M' [L]_T} \cdot \frac{1}{[M]_T} \quad (8)$$

(ii) Cu^{2+} Catalysis. As suggested in Figs. 2 and 4, the active complex of a bis-imidazole · Cu^{2+} is M–L, but the M–L_2 is inactive. Then it can be assumed that under the conditions of $[M]_T \gg [L]_T$=constant, the complex concentration at the rate saturation, [M–L](max), is equal to the total concentration of ligand, $[L]_T$, and thus the saturated rate, k_{obsd}(max), is represented by Eq. 9.

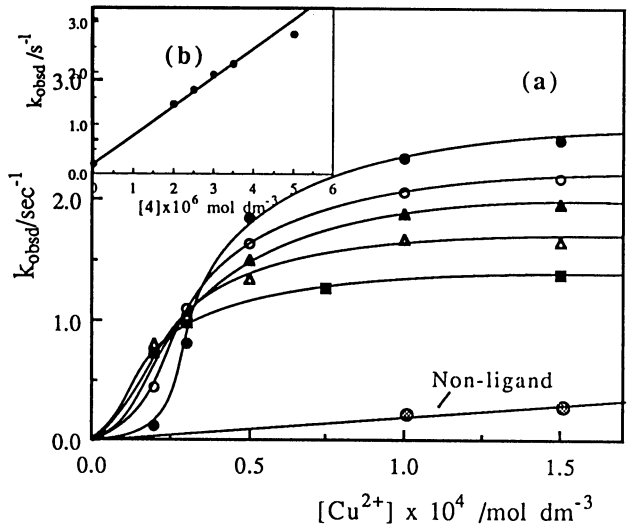

Fig. 9. Plots of k_{obsd} vs. Cu^{2+} concentration for *p*-nitrophenol release from PNPP in HTAB micelles (1×10^{-2} mol dm^{-3}), pH 7.03, 25 °C: ligand **4** concentrations are 5.0, 3.5, 3.0, 2.5, and 2.0×10^{-5} mol dm^{-3} from the top curve (a). Inside figure (b) shows a plot of k_{obsd} vs. ligand **4** concentration at the rate saturation: $Cu^{2+}=1.5\times10^{-4}$ mol dm^{-3} for the lower 5 points and 5×10^{-4} mol dm^{-3} for the upper one.

These assumptions are supported by the saturation kinetics shown in Fig. 9a and the resulting linear plot in Fig. 9b, which allows to obtain k_N' as the slope. Unfortunately, it is difficult to determine the association constant K_M, only it is estimated from the saturation curves in Fig. 9a to be around 4×10^4 mol dm^{-3} for **4**.

In the case of **2**·Cu^{2+} complex, the active complex was found to be a 2 : 1 complex (n=2), the same as in the case of **1**·Cu^{2+} complex, and the corresponding k_N and K_M values were obtained similarly as before.[13]

$$k_{obsd}(max) = k_0' + k_N'[M\text{-}L](max)$$
$$= k_0' + k_N'[L]_T; \qquad M]_T \gg [L]_T \qquad (9)$$

(d) pH-Rate Profiles. The above mentioned k_N' and K_M' values should be pH dependent if the active complex is a dissociated complex anion (A^-) as illustrated in Scheme 3. The acylation rate constant k_N for the fully dissociated hydroxyl group of the complex and its acid dissociation constants K_a can be obtained based on the relationship between Eqs. 10 and 11.

$$k_{N'} = \frac{k_N K_a}{K_a + [H^+]} \qquad (10)$$

$$\frac{1}{k_{N'}} = \frac{1}{k_N} + \frac{1}{k_N K_a}\cdot[H^+] \qquad (11)$$

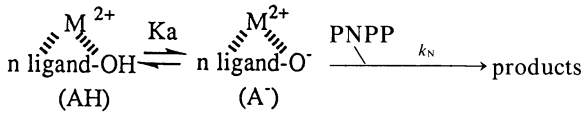

$$[M\text{-}L_n]_T = [AH] + [A^-]$$

Scheme 3.

As shown in Figs. 10 and 11, the $\log k_N'$ values increased linearly with a slope of 1 with increasing pH, except for the plot of **6**·Zn^{2+} in Fig. 11: They then became pH independent at higher pH. These pH-rate profiles can be accounted for by assuming that the dissociated complex anion (A^- in Scheme 3) is much more active than the undissociated complex (AH). Then, the pK_a's of AH and the k_N values for A^- could be calculated from the plots of $1/k_N'$ vs. [H^+] based on Eq. 11. The combined results on k_N, K_a, and K_M are summarized in Table 2. The table indicates for the bis-imidazole ligands that the pK_a's of the secondary hydroxyl groups complexed with Zn^{2+} are 7.5 (**4**) and 8.1 (**3**), and those of the primary hydroxyl groups complexed with Cu^{2+} are 6.1 (**4**) and 6.3 (**6**), respectively. It also indicates for the monoimidazole ligands that the pK_a's of the primary hydroxyl groups complexed with

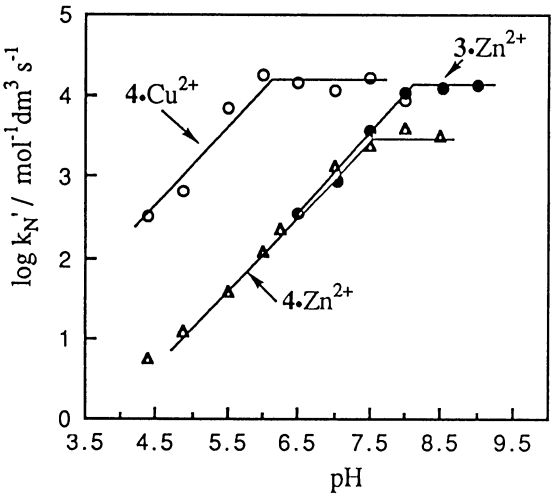

Fig. 10. pH-Rate profiles for the acylation rate constant k_N' for the metal ion complexes of ligand **3** and **4** in HTAB micelles, 25 °C.

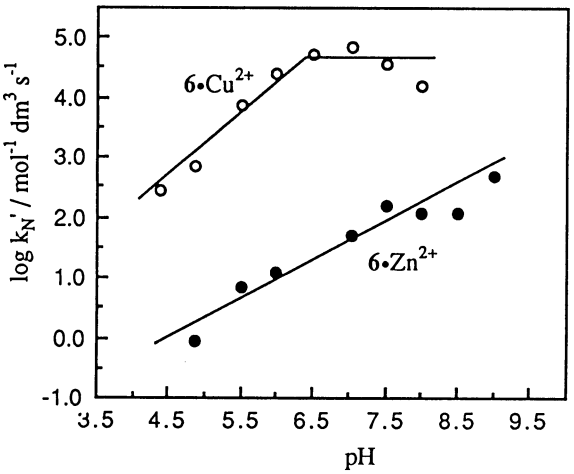

Fig. 11. pH-Rate profiles for the acylation rate constant k_N' for the metal ion complex of ligand **6** in HTAB micelles, 25 °C.

Table 2. Kinetic Parameters for *p*-Nitrophenol Release from PNPP Catalyzed by Metal Ion Complexes of Lipophilic Imidazole Ligands in HTAB Micelle

Ligand	Metal ion	pK_a of lig-OH	k_N / $mol^{-1}\,dm^3\,s^{-1}$	K_M (pH 7.0)	Ref.
1	Cu^{2+}	6.41	1.25×10^6	9.3×10^7 $mol^{-2}\,dm^6$	Ref. 13
2	Cu^{2+}	6.78	4.90×10^5	4.1×10^7 $mol^{-2}\,dm^6$	This work
3	Zn^{2+}	8.10	1.31×10^4	2.6×10^4 $mol^{-1}\,dm^3$	Ref. 9
4	Zn^{2+}	7.5	3.88×10^3	1.3×10^4 $mol^{-1}\,dm^3$	This work
	Cu^{2+}	6.1	1.67×10^4	—	This work
6	Cu^{2+}	6.3	3.68×10^4	—	This work

Cu^{2+} are 6.41 (**1**) and 6.78 (**2**), respectively, although the corresponding pK_a values could not be determined for the Zn^{2+} complexes because of their instability at higher pH. Thus the pK_a's of Cu^{2+} complexes are 1—2 units lower than those of the Zn^{2+} complexes. Furthermore, it is interesting to notice that the activity (k_N) of Zn^{2+} complexes of **3** and **4** are comparable with those of the Cu^{2+} complexes of **4** and **6** within ten fold rate difference. The difference between **4**·Zn^{2+} (Fig. 10) and **6**·Zn^{2+} (Fig. 11) in both the magnitude of k_N' value and the slope of pH-rate profile suggests that Zn^{2+} activates the secondary hydroxyl group by site-selective coordination (see also Fig. 3).

Burst Kinetics. The above k_N value is the rate constant for the release of *p*-nitrophenol, i.e. that for the acylation step. For an efficient catalysis to occur, the deacylation step must also be fast. Fig. 12 indicates how fast and how much *p*-nitrophenol was produced under the conditions of an excess PNPP over the ligand **4**. The curves a and b show that each ten and five molar excess PNPP was rapidly hydrolyzed in the presence of 2×10^{-5} mol dm^{-3} of **4** and 1×10^{-4} mol dm^{-3} of Cu^{2+}, respectively. With a less amount of Cu^{2+}, a biphasic burst curve c became apparent to indicate a two step process. At any rate, in the presence of enough amount of Cu^{2+}, **4** behaves as an efficient catalyst in both acylation and deacylation steps. In the cases of Zn^{2+}, the curves d and e were of typical burst kinetics, indicating that the acylation is fast but the deacylation is relatively slow. The amount of *p*-nitrophenol obtained by extrapolating the steady-state lines of d and e to time=0 corresponds roughly to the amount of ligand (2×10^{-5} mol dm^{-3}) employed, which means only one

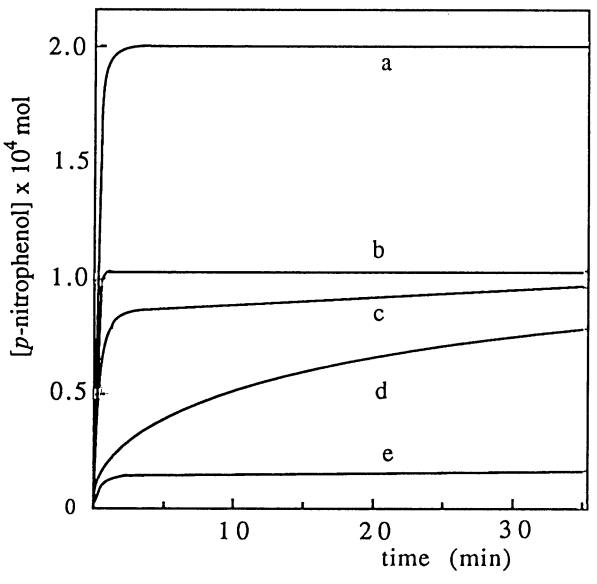

Fig. 12. Effect of Zn^{2+} or Cu^{2+} with ligand **4** (2×10^{-5} mol dm^{-3}) on the time-dependent release of *p*-nitrophenol from PNPP under the conditions of [PNPP]≫[**4**] in HTAB micelles (1×10^{-2} mol dm^{-3}), pH 7.03, 25 °C: Cu^{2+} or Zn^{2+} (mol dm^{-3}) and [PNPP]/[**4**] are (a) Cu^{2+} (1×10^{-4}) and 10, (b) Cu^{2+} (1×10^{-4}) and 5, (c) Cu^{2+} (4×10^{-5}) and 5, (d) Zn^{2+} (1×10^{-4}) and 5, (e) Zn^{2+} (1×10^{-5}) and 5.

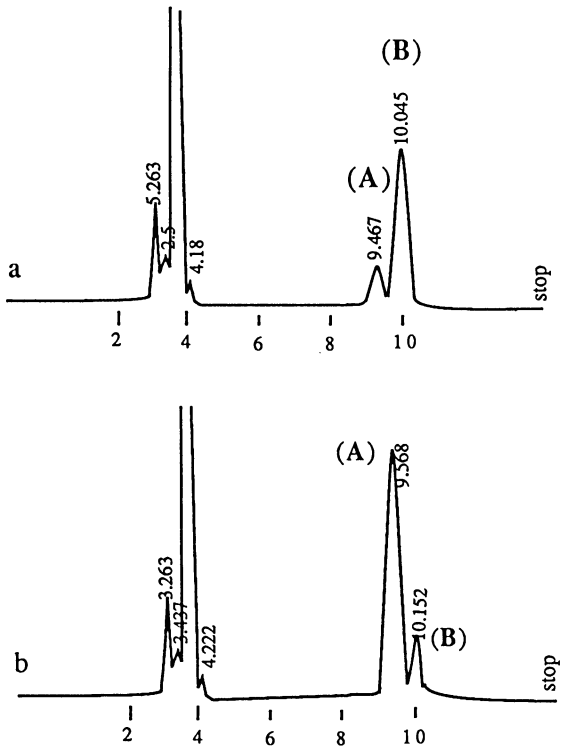

Fig. 13. HPLC chromatograms of the reaction mixtures of PNPP and ligand **4** (1×10^{-4} mol dm^{-3}) in the presence of (a) Zn^{2+} (2×10^{-2} mol dm^{-3}) and (b) Cu^{2+} (2×10^{-2} mol dm^{-3}) in HTAB micelles (1×10^{-2} mol dm^{-3}): after one minute reaction, pH 7.0, 25 °C. Column: Shimpack CLC-ODS, Eluent: methanol, Flow rate: 0.8 mL min^{-1} Detecter: UV (300 nm).

hydroxyl group being acylated. In the present study, further attempt to determine the deacylation rate constant for **4** was not undertaken because of the expected difficulty in a complete separation of the two hydroxyl groups in reactivity. In the case of ligand **3** with Zn^{2+}, it was shown previously that the deacylation step becomes much faster by raising the concentration of Zn^{2+} and pH, and the deacylation rate constant k_d could be determined at pH 8.[9]

Site-Selective Acylation. (a) Analysis of Intermediate Products. The above metal ion dependent site-selective activation of hydroxyl groups of **4** demonstrated by kinetic means (Figs. 3 and 4) was further confirmed by the product analysis. A typical product analysis by HPLC is shown in Fig. 13 which was obtained by analyzing a reaction mixture, after one minute reaction (25 °C, pH 7). The figure indicates two peaks A and B. Although the relative peak area of these A and B was dependent on the reaction time, the predominant peak at the initial stage was A in the presence of Zn^{2+}, while that was B in the presence of Cu^{2+}. These products A and B could be prepared by the separate reactions of **4** with PNPP in a two-phase media, in the presence of zinc nitrate for A and copper nitrate for B, respectively (see experimental).

The structures of the above A and B were assigned to those of **12** and **13** by assuming that the acylation should cause the largest change in the NMR chemical shift of the acylated hydroxyl group. The ^{13}C resonance peaks of the free ligands **1**, **2**, and **3** appeared at δ=57.6^t ($-CH_2OH$), 55.4^t ($-CH_2OH$), and 65.0^d (〉CHOH), respectively, whereas those of the acylated products **9**, **10**, and **11** appeared at δ=58.2^t ($-CH_2O$acyl), 61.7^t ($-CH_2O$acyl), and 56.5^d (〉CHOacyl), respectively. Although there is a difference in the direction of change in such way that the acylation of the former two primary hydroxyl groups resulted in a downfield shift, but an upfield shift in the acylation of the latter secondary hydroxyl group. The changes in the chemical shifts of the other peaks were relatively small upon the acylation.

The free ligand **4** showed the ^{13}C peaks at 58.1^t ($-CH_2OH$) and 64.5^d (〉CHOH). The above product A showed the ^{13}C peaks at δ=58.6^t and 57.4^d, while the product B showed the corresponding peaks at 61.4^t and 71.1^d. Thus, in A an upfield shift is seen between the peaks of secondary hydroxyl group (doublet peaks) with a very small change between the peaks of primary hydroxyl group (triplet peaks) indicating A being **12**. Contrary, a downfield shift is seen in B between the peaks of primary hydroxyl group (triplet peaks) indicating B being **13**, although a sizable downfield shift is also seen between the peaks of secondary hydroxyl group (doublet peaks).

The ^1H NMR specra were examined similarly. In all the ligands, **1**, **2**, and **3**, the acylation caused a downfield shift of methylene or methyne proton-peak. The ^1H signals of the free ligand **4** appear at δ=4.48^s ($-CH_2O-$) and 6.03^s (〉CHO–). The product A showed the peaks at δ=4.51^s and 6.81^s, and the product B showed the corresponding peaks at δ=5.85^s and 6.10^s, respectively. Thus, in A a downfield shift is much larger for the latter secondary hydroxyl methyne proton than for the former primary methylene protons indicating A being **12**, whereas in B an opposite trend is observed indicating B being **13**.

(b) Time Dependent Distribution of Intermediates. Figs. 14 and 15 indicate that under the conditions of an excess PNPP over the ligand **4**, the distribution of intermediates **12** and **13** was found to be time dependent. It is seen in Fig. 14 that in the presence of Zn^{2+} the initial product was predominantly **12** in consistent with the result in Fig. 13a, but followed with an increase of **13** after some time lag to give almost an equal mixture of **12**

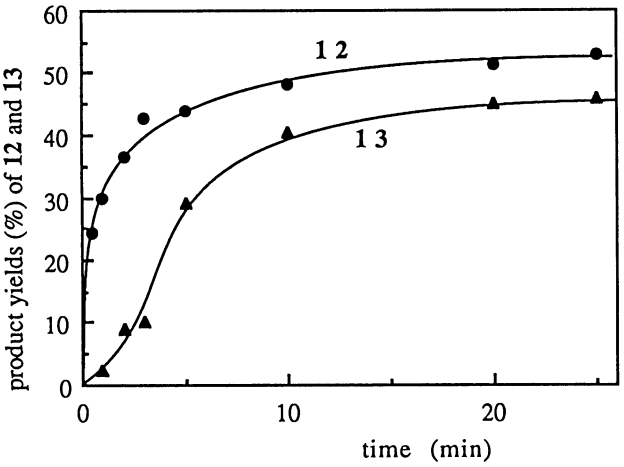

Fig. 14. Time course of product distribution in the reaction mixture of PNPP (3×10^{-4} mol dm^{-3}) with ligand **4** (1×10^{-4} mol dm^{-3}) in the presence of Zn^{2+} (2×10^{-4} mol dm^{-3}) in HTAB micelles (1×10^{-2} mol dm^{-3}), pH 7.03, 25 °C.

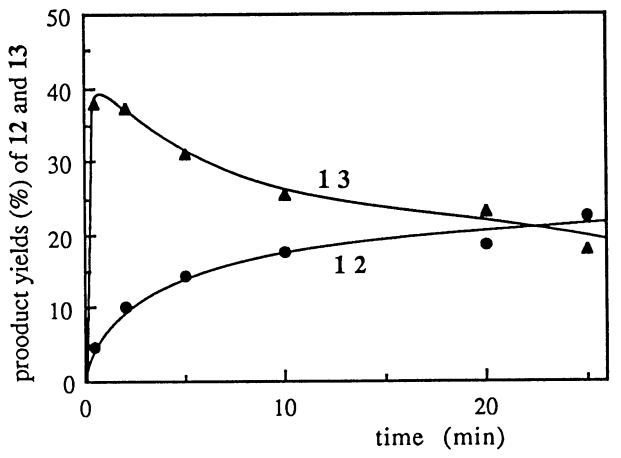

Fig. 15. Time course of product distribution in the reaction mixture of PNPP (3×10^{-4} mol dm^{-3}) with ligand **4** (1×10^{-4} mol dm^{-3}) in the presence of Cu^{2+} (2×10^{-4} mol dm^{-3}) in HTAB micelles (1×10^{-2} mol dm^{-3}), pH 7.03, 25 °C.

and **13**, with their combined yield of 99% which indicates the deacylation being very slow as compared to the acylation. It is seen in Fig. 15 that in the presence of Cu^{2+} the initial product was predominantly **13**, also in consistent with the result in Fig. 13b, but followed with an increase of **12** and with a concomitant decrease of **13**. Here an equal mixture of **12** and **13** is also obtained after about 20 min, but their total yield was about 40% indicating the deacylation being fairly fast (Fig. 12). Both **12** and **13** are the monoacylated products and any trace of diacylated product **14** could not be detected. This observation appears to be important for the consideration of the mechanism of the isomerization between **12** and **13** described below.

(c) Isomerization between the Intermediates 12 and 13. As mentioned above, the initial site selective acylation of **4** was lost along with the progress of reaction. Two possibilities are conceivable. The first possibility is that the minor acylated intermediate would accumulate if its deacylation rate to regenerate the free ligand is slower than that of the major acylated intermediate, i.e. the Zn^{2+} catalyzed deacylation of **13** (the minor product) is slower than that of **12** (the major product) and the Cu^{2+} catalyzed deacylation of **12** (the minor product) is slower than that of **13** (the major product). The second possibility is an intramolecular and/or intermolecular acyl migration between primary and secondary hydroxyl groups. In order to obtain more information, the deacylation and/or the isomerization of **13** was further examined.

As shown in Fig. 16, **13** was rapidly disappeared in the presence of Cu^{2+} with a concomitant rapid appearence of **12**, which indicates that most of **13** was transformed into **12** prior to the hydrolysis. Although with much slower rate, similar isomerization was also effected by Zn^{2+} as shown in Fig. 17. It was verified that **13** was stable in the absence of Cu^{2+} or Zn^{2+}. Then, how can such a M^{2+} catalyze or promote the isomerization of **13** to **12**? Examination by CPK molecular model reveals that an intramolecular migration of PyCO group from the primary hydroxyl group to the secondary one and vice versa is impossible because of the too remote distance between the two hydroxyl groups in any possible conformations. Therefore, some mechanism of intermolecular isomerization must be considered. One possibility is a pseudo-intramolecular acyl group migration within a dimeric copper complex of **13**. As illustrated in Scheme 4, with CPK molecular models it is possible to set up an octahedral M^{2+} complex of dimeric **13 A**, in which the two imidazole nitrogen atoms and the two oxygen atoms of secondary hydroxyl groups occupy equatorial positions and the two pyridine nitrogen atoms occupy the axial positions, and the secondary hydroxyl group of one molecule coordinated to M^{2+} is in close proximity of the carbonyl carbon of the other molecule. It is also possible to set up a tetrahedral addition intermediate **B** which would be formed from **A** and collapse to the isomer **12**. In Scheme 4, it is

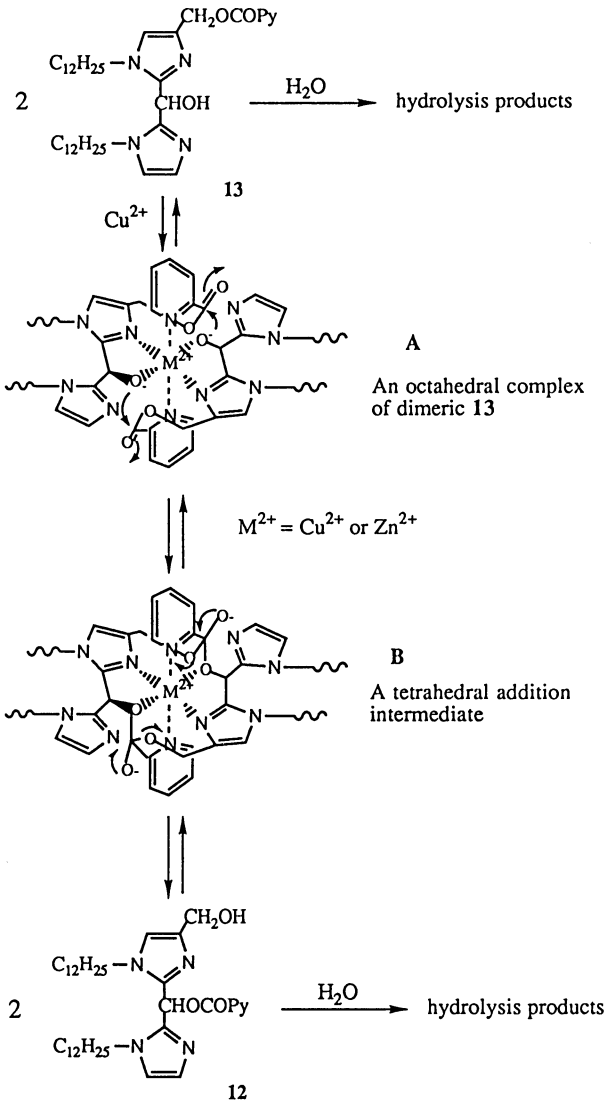

Scheme 4. A possible mechanism of the isomerization of **13** to **12**.

assumed that the two acyl groups migrate at the same time, although other possibilities such as a stepwise migration of one acyl group followed by the other might also be conceivable. The reason why the latter possibility is omitted is simply due to the failure of detection of the diacylated product **14** which would be expected for a stepwise migration. According to Scheme 4, the isomerization between **12** and **13** must be an equilibrium process, but the isomerization of **12** to **13** was not observed as can be anticipated from the result shown in Fig. 16, i.e. the equilibrium being heavily balanced to **12**.

Conclusions. As described above, it has been demonstrated for a bis-imidazole ligand **4** that the primary and secondary hydroxyl groups are selectively activated by Cu^{2+} and Zn^{2+}, respectively, for the acylation with PNPP. As illustrated in Fig. 18, such selectivity seems to be nicely explained by assuming a tetrahedral geometry for the ternary complex of **4**-Zn^{2+}–PNPP (**a**) and a square planar one for the complex of **4**-Cu^{2+}–PNPP (**b**)

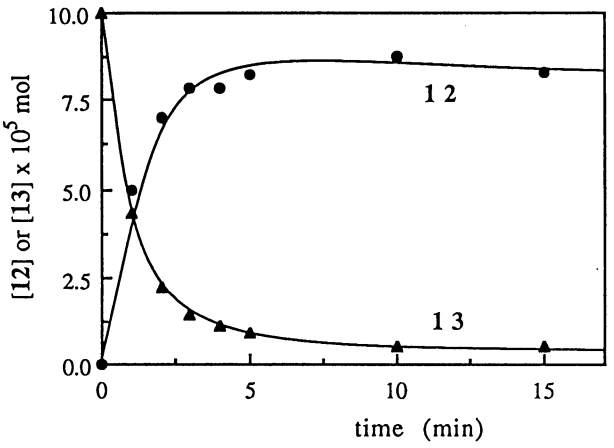

Fig. 16. Time course of the Cu^{2+} (2×10^{-4} mol dm^{-3}) promoted isomerization between the acylated ligands **13** (▲; 1×10^{-4} mol dm^{-3}) and **12** (●) in HTAB micelles (1×10^{-2} mol dm^{-3}), pH 7.03, 25 °C.

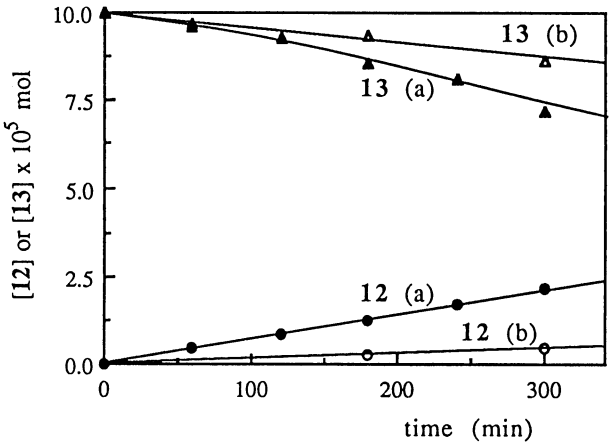

Fig. 17. Time course of the Zn^{2+} promoted isomerization between the acylated ligands **13** (△, ▲: 1×10^{-4} mol dm^{-3}) and **12** (○, ●) in HTAB micelles (1×10^{-2} mol dm^{-3}), pH 7.03, 25 °C: Zn^{2+} concentration are (a) 2×10^{-4} and (b) 1×10^{-3} mol dm^{-3}.

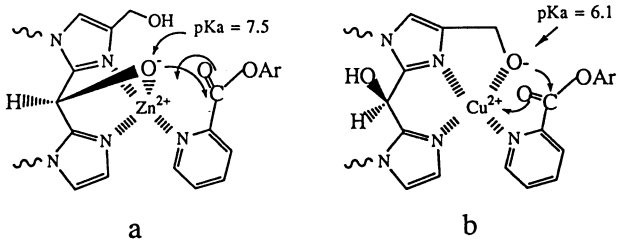

Fig. 18. Schematic illustration of selective activation of primary and secondary hydroxyl groups of bis-imidazole ligand **4** by Zn^{2+} (**a**) and Cu^{2+} (**b**), respectively, in HTAB micelles.

for the transition states or the reactive intermediates. In **18a**, the CPK molecular model indicates that the oxygen atom of secondary hydroxyl group coordinates tightly to Zn^{2+}, while the oxygen atom of the primary hydroxyl group is positioned away from Zn^{2+} without touching. Contrary, in **18b**, the oxygen atom of primary hydroxyl group coordinates tightly to Cu^{2+}, while the oxygen atom of secondary hydroxyl group is positioned away from Cu^{2+} without contact. The tight coordination with an electrophilic metal ion facilitates the ionization of hydroxyl groups to result in remarkable lowering of their pK_a (=6—8 in Table 2). Thus such coordinated ligand hydroxyl groups are fully dissociated in neutral aqueous media, retaining high nucleophilic reactivities. These findings present critical information how to design a ligand for a particular metal ion and to develope more efficient artificial enzymes.

Finally, the present study has disclosed several interesting problems which ought to be solved. In particular, the mechanism of an efficient catalysis by **4**-Cu^{2+} complex in the deacylation step must be clarified. It is also interesting to elucidate the detailed mechanism of isomerization between **12** and **13**, since the mechanism in Scheme 4 is only of a tentative proposal.

Experimental

Materials. The water used for kinetics was obtained by distilling deionized water twice. Acetonitrile was purified by distillation over P_4O_{10}. Commercially available 2,6-lutidine, *N*-ethylmorpholine, and acetic acid were purified prior to use by distillation. Commercially available extra-pure $Zn(NO_3)_2\cdot H_2O$ and $Cu(NO_3)_2\cdot6H_2O$ were used without further purification. Other inorganic salts used for buffer preparation were also commercial extra-pure reagents. HTAB was recrystallized from acetonitrile before use. The buffers were CH_3COOH/CH_3COONa (pH 4.46—4.97), 2,6-lutidine/HNO_3 (pH 5.50—6.50), and *N*-ethylmorpholine/HNO_3 (pH 7.03—8.00), and the ionic strength was maintained at 0.2 mol dm^{-3} with NaCl (pH 4.46—4.97) or with KNO_3 (pH 5.50—8.00). PNPP was prepared and purified according to previous methods.[7] PNPP stock solutions for kinetics were prepared in acetonitrile. 1-Dodecyl-2-hydroxymethylimidazole (**1**),[10] 1-dodecyl-4-hydroxymethylimidazole (**2**),[10] and bis(1-octyl-2-imidazolyl)methanol (**3**)[11] reported previously showed the following spectral data. ^{13}C NMR ($CDCl_3$, 60 MHz); **1**, δ=14.1^q, 22.7^t, 26.5^t, 29.0^t, 29.3^t, 29.4^t, 29.6^t, 30.9^t, 31.8^t, 47.1^t, 57.6^t, 116.1^d, 136.6^d, 142.6^s; **2**, δ=14.1^q 22.7^t, 26.7^t, 29.2^t, 29.3^t, 31.0^t, 31.9^t, 40.1^t, 55.4^t, 119.6^d, 126.5^d, 147.8^s; **3**, δ=14.1^q, 22.7^t, 26.6^t, 29.2^t, 30.2^t, 31.8^t, 46.2^t, 65.0^d, 120.9^d, 127.0^d, and 145.7^s.

1-Dodecyl-4-hydroxymethyl-α-(1-dodcyl-2-imidazolyl)-2-imidazolemethanol (4). A solution of 1-dodecylimidazole (9.44 g, 40 mmol) in 100 mL of dry THF was cooled to −70 °C under nitrogen and 2.1 M butyllithium in hexane (30 mL, 63 mmol) was added over 10 min via syringe. After 1.5 h stirring at this temperature, dry DMF (5 g, 70 mmol) was added at once. The reaction mixture was allowed to warm slowly and quenched with water. Chromatographic separation (Wako gel C-200, eluted with chloroform–methanol 50 : 1) and evaporation of the solvent afforded 1-dodecyl-2-formylimidazole (**7**) (9.02 g, 80% yield) as an oil. To a mixture of 1-dodecyl-4-hydroxymethylimidazole (**2**) (8.6 g, 32 mmol) and *p*-toluenesulfonic acid (8.3 g, 48 mmol) in 100 mL of dry dichloromethane was added 3,4-dihydro-2*H*-pyran (8.4

g, 100 mmol) at 0—5 °C with stirring for 2 h. The resulting solution was neutralized by addition of 2 M (1 M=1 mol dm^{-3}) sodium hydroxide solution and extracted with methylene chloride. After evaporation of the solvent, the remaining material was purified by a column chromatography (Wako gel C-200, eluted with chloroform–methanol 50 : 1). The protected imidazole **8** was obtained as an oil (10.3 g, 91%). This protected imidazole **8** (10.3 g, 29 mmol) was metalated in 100 mL of THF with 2.1 M butyllithium in hexane (16 mL, 34 mmol) at −70 °C under nitrogen, and 1-dodecyl-2-formylimidazole (**7**) (7.67 g, 29 mmol) in 30 mL of THF was added dropwise with stirring. The reaction mixture was allowed to stand for overnight and quenched with water. After evaporation of the solvent, to the remaining oily product 100 mL of methanol and *p*-toluenesulfonic acid-monohydrate (19 g, 0.1 mol) was added with stirring at room temperature to remove the protecting group. After 2 h the mixture was neutralized with 2 M sodium hydroxide, concentrated to remove methanol and the residue was extracted with dichloromethane. The oily residue after removal of the solvent was purified by a column chromatography (Wako gel C-200, eluted with chroloform–ethanol 20 : 1). The product was crystallized from diethyl ether–acetonitrile to give bis-imidazole **4** (4.87 g, 32% yield) as a white powder; mp 72—75 °C, ^{1}H NMR ($CDCl_3$, 100 MHz) δ=0.89 (t, J=6 Hz, 6H), 1.27 (br s, 40H), 3.80 (t. J=7 Hz, 4H), 4.46 (s, 2H), 4.80 (br s, 2H), 6.01 (s, 1H), and 6.73—6.88 (m, 3H); ^{13}C NMR ($CDCl_3$, 60 MHz) δ=14,1^q, 22.7^t, 26.6^t, 29.2^t, 29.3^t, 29.6^t, 30.7^t, 30.8^t, 31.9^t, 46.1^t, 58.1^t, 64.5^d, 118.0^d, 120.8^d, 126.9^d, 140.0^s, 145.5^s, and 145.6^s. Found: C, 72.3; H, 10.8; N, 10.7%. Calcd for $C_{32}H_{58}O_2N_4$: C, 72.4; H, 10.9; N, 10.6%.

The protected ligand **5** was obtained and purified before the removal of tetrahydropyranyl group to give **4**. The another protected ligand **6** was obtained by methylation of **5** followed by removal of tetrahydropyranyl group. These ligands **5** and **6** have similar NMR spectra as those of **4** with the additional tetrahydropyranyl (δ=1.7—2.1 (m, 4H), 3.6—4.0 (m, 2H), and 5.0—5.3 (m, 1H)) or methyl (δ=3.40 (s, 3H)) signal.

Kinetics. Kinetics were carried out according to essentially the same method as reported previously.[10–13] A Hitachi-Horiba pH meter F-8 was used for the pH determination and control. The kinetic runs for slow rates were conducted by using either a Hitachi 220 or 220A spectrophotometer equipped with a thermostated cell compartment. They were initiated by introducing a 10 μl of the PNPP stock solution into a 3 mL of a buffer solution containing the desired reagents. Kinetic runs for fast rates were conducted by using a Union Giken RA-401 stopped-flow spectrophotometer equipped with an RA-454 thermobath and an RA-451 computer. The PNPP stock solution was diluted by a buffer before use. The reactions were initiated by mixing an equal volume of PNPP buffer and the desired reagent solutions. In both slow and fast reactions, the rates were followed by monitoring the release of *p*-nitrophenol at 400 nm (pH 6.5—8.0) or at 320 nm (pH 4.5—6.0). The kinetic runs used for the calculation of rate constants obeyed the pseudo-first-order kinetics for at least 3 half-lives. The absorbance at infinite time (OD_∞) was recorded for each run, and the pseudo-first-order rate constants were obtained by using $k_{obsd}=(2.30/t)\log[(OD_\infty-OD_0)/(OD_\infty-OD_t)]$. The graphical methods for the analyses of these k_{obsd} to obtain k_N', k_M, k_N, and K_a are described in the text (Eqs. 6—11).

Product Analyses by HPLC. The product analyses were performed by high-pressure liquid chromatography (HPLC) using a Shimadzu Model LC-6A/G-I system equipped with a Shimpack CLC-ODS reverse phase column with the elution solvent of methanol–water 19 : 1.

a) Typical Run. The bulk micellar solution for the reaction mixture was composed of *N*-ethylmorpholine/HNO_3 0.1 mol dm^{-3}, pH 7.0), KNO_3 (μ=0.2), and HTAB (0.01 mol dm^{-3}) in deionized and distilled water. The reaction was initiated by injecting 100 μL of PNPP stock solution (0.75 mol dm^{-3} in acetonitrile) into 25 mL of the HTAB micellar solution containing 0.01 mmol of the ligand **4** and 0.02 mmol of Zn^{2+} or Cu^{2+} at room temperature. After 1 min, the mixture was quenched with a stirring mixture of 30 mL of chloroform and 10 mL of water containing 2.0 g of ethylenediaminetetraacetic acid (EDTA) to deactivate the metal ion. Extraction of the quenched mixture with chloroform, drying of chloroform layer (Na_2SO_4), and evaporation of the chloroform gave a partially oily residue. This crude product was dissolved in 5 mL of methanol containing 1×10^{-6} mol dm^{-3} of diphenyl disulfide (an internal standard) and subjected for a HPLC analysis. The resulting chromatograms are shown in Fig. 13.

b) Time Courses of Product Distribution. The time courses of the product distribution were followed similarly as shown in Figs. 14 and 15.

c) Product Isolation for NMR Analysis. The reaction was carried out in two phase system: The ligand **4** (0.1 g, 0.88 mmol) and PNPP (68.9 mg, 0.282 mmol) in 15 mL of dichloromethane was mixed with Zn^{2+} or Cu^{2+} (0.282 mmol) in 10 mL of water with stirring at room temperature. After the disappearance of PNPP, the reaction mixture was quenched with 20 mL of water containing EDTA (2.5 g), and the methylene chloride layer was treated for product isolation. The crude product was purified with chromatography on silica gel (eluted with chloroform–methanol 20 : 1) to give an analytical sample. The ^{13}C NMR ($CDCl_3$, 60 MHz) signals of the acylated products appeared as follows; **9**, δ=14.1^q, 22.7^t, 26.7^t, 29.2^t, 29.3^t, 31.1^t, 31.8^t, 46.4^t, 58.2^t, 120.9^d, 125.2^d, 127.0^d, 128.4^d, 136.9^d, 141.5^s, 147.4^s, 149.9^d, and 164.4^s; **10**, δ=14.1^q, 22.7^t, 26.5^t, 29.0^t, 29.4^t, 29.6^t, 30.9^t, 31.8^t, 47.1^t, 61.7^t, 119.1^d, 125.2^d, 126.6^d, 136.8^s, 148.2^s, 149.8^d, and 164.9^s; **11**, 14.1^q, 24.6^t, 25.5^t, 26.3^t, 30.8^t, 32.5^t, 49.8^t, 56.5^d, 122.9^d, 125.0^d, 136.9^d, 142.5^s, 148.4^d, 153.9^s, and 168.1^s. The main product **12** of the reaction of **4** with PNPP in the presence of Zn^{2+}, corresponding to the peak A in Fig. 13, had ^{13}C NMR ($CDCl_3$) δ=14.1, 22.7, 25.3, 26.7, 29.3, 29.6, 30.9, 31.6, 31.9, 34.6, 46.3, 46.5, 57.4^d, 58.6^t, 117.9, 120.8, 127.0, 127.6, 128.1, 136.8, 140.3, 141.7, 143.2, 143.4, 149.8, and 163.5; IR (KBr disk) 1725 cm^{-1} (ester). The main product **13** of the reaction in the presence of Cu^{2+}, corresponding to the peak B, showed ^{13}C NMR ($CDCl_3$) δ=14.1, 22.7, 26.7, 29.2, 29.3 29.6, 30.8, 46.7, 61.4^t, 71.1^d, 115.3, 121.8, 125.1, 125.9, 126.8, 135.7, 136.8, 141.5, 142.3, 148.0, 149.8, and 164.9; IR (KBr disk) 1720 cm^{-1} (ester).

This work was partly supported by a Grant-in-Aid from the Ministry of Education, Science and Culture: Special project research (Supramolecular Assemblies, 1986—1989).

References

1) J. A. Hartsuck and W. N. Lipscomb, in "The Enzymes," 3rd ed, ed by P. D. Boyer, Academic Press, New York (1971),

Vol. 3, Chap. 1, pp. 11—12.

2) T. W. Reid and I. B. Wilson, in "the Enzymes," 3rd ed, ed by P. D. Boyer, Academic Press, New York (1971), Vol. 4, Chapt. 17, pp. 373—415.

3) S. Lindskog, L. E. Henderson, K. K. Kannan, A. Liljas, P. O. Nyman, and B. Strandberg, in "The Enzymes," 3rd ed, ed dy P. D. Boyer, Academic Press, New York (1971), Vol. V, pp. 587—665.

4) A. Fersht, "Enzyme Structure and Mechanism," 2nd ed, W. H. Freeman, New York (1985).

5) R. B. Martin, *J. Inorg. Chem.*, **38**, 511 (1976).

6) L. M. Sayer, *J. Am. Chem. Soc.*, **108**, 1632 (1986), and the references therein.

7) D. S. Sigman and C. T. Jorgensen, *J. Am. Chem. Soc.*, **94**, 1724 (1972); K. Ogino, K. Shindo, T. Minami, W. Tagaki, and T. Eiki, *Bull. Chem. Soc. Jpn.*, **56**, 1101 (1983); R. S. Brown, M. Zamkanei, and J. L. Cocho, *J. Am. Chem. Soc.*, **106**, 5222 (1984); S. H. Gelman, R. Petter, and R. Breslow, *ibid.*, **108**, 2388 (1986); R. Breslow and A. Schepartz, *ibid.*, **109**, 1814 (1987); J. T. Groves and L. A. Baron, *ibid.*, **111**, 5442 (1989).

8) J. Chin, *Acc. Chem. Res.*, **24**, 145 (1991), and the references therein.

9) W. Tagaki and K. Ogino, *Top. Curr. Chem.*, **128**, 143 (1985).

10) T. Eiki, M. Mori, S. Kawada, K. Matsushima, and W. Tagaki, *Chem. Lett.*, **1980**, 1431.

11) a) K. Ogino, I. Tomita, K. Machiya, and W. Tagaki, *Chem. Lett.*, **1982**, 1875; b) T. Fujita, H. Minami, K. Ogino, and W. Tagaki, *ibid.*, **1987**, 2289; c) T. Fujita, K. Ogino, and W. Tagaki, *ibid.*, **1988**, 981; d) T. Fujita, Y. Inaba, K. Ogino, and W. Tagaki, *Bull. Chem. Soc. Jpn.*, **61**, 1661 (1988).

12) K. Ogino, N. Kashihara, T. Fujita, T. Ueda, T. Isaka, and W. Tagaki, *Chem. Lett.*, **1987**, 1303.

13) W. Tagaki, K. Ogino, O. Tanaka, K. Machiya, N. Kashihara, and T. Yoshida, *Bull. Chem. Soc. Jpn.*, **64**, 74 (1991).

14) R. Fornasier, D. Milani, and U. Tonellato, *J. Chem. Soc., Perkin Trans. 2*, **1986**, 223; R. Fornasier, P. Scrimin, P. Tecilla, and U. Tonellato, *J. Am. Chem. Soc.*, **111**, 224 (1989); T. Kuwamura, Y. Yano, S. Inokuma, Y. Takenouchi, and H. Tokue, *Chem. Lett.*, **1986**, 1519; F. M. Menger, L. H. Gan, E. Johnson, and D. H. Durst, *J. Am. Chem. Soc.*, **109**, 2800 (1987).

15) Part of the results were reported in a previous communication (Ref. 12).

16) A. Martell and S. Chabarek, "Organic Sequestering Agents," Wiley, New York (1959).